ISSN 0915-633X

NATIONAL INSTITUTE FOR FUSION SCIENCE

Symmetry-Breaking due to Parallel Electron Motion and Resultant Scaling in Collisionless Magnetic Reconnection

M. Tanaka and D. Biskamp

(Received - Feb. 21, 1996)

NIFS-406 Mar. 1996

RESEARCH REPORT
NIFS Series

NAGOYA, JAPAN

Symmetry-Breaking due to Parallel Electron Motion and Resultant Scaling in Collisionless Magnetic Reconnection

Motohiko Tanaka, and Dieter Biskamp*

National Institute for Fusion Science, Nagoya 464-01, Japan
*Max-Planck Institüt für Plasmaphysik, D-85748 Garching, Germany

Abstract

The macro-particle simulations of magnetically reconnecting flux bundles in a collisionless magnetized plasma show a remarkable asymmetry of the poloidal flow. The corresponding current for the electron and ion species has a significant divergence, $\nabla_{\parallel} \cdot \mathbf{J}_{\parallel}^{(e)} \neq 0$ and $\nabla_{\perp} \cdot \mathbf{J}_{\perp}^{(i)} \neq 0$, which creates substantial density inhomogeneity and toroidal magnetic field to result in a thick current sheet. The reconnection rate is found to increase mildly with increasing ion mass or decreasing the toroidal magnetic field, but to decrease drastically for ion Larmor radii comparable to the ion skin depth.

Keywords: flow asymmetry, electron parallel dynamics,
finite Larmor radius effect, implicit particle simulation.

§1. Introduction

The formation of a current sheet and its micro-structure are fundamental issues of magnetic reconnection in collisionless plasmas, since they will essentially determine the reconnection speed. To investigate such processes, we need to use collisionless MHD equations or particle simulations instead of resistive MHD equations. Previous studies of collisionless reconnection along two-fluid theory showed that the current sheet at the interface between the flux bundles collapsed to virtually zero thickness[1-3]. For symmetric initial conditions, the coalescence process remained completely symmetric. By contrast, the macro-particle simulations show a significant asymmetry of the electron flow in the current sheet[4] and a highly compressed neutral sheet with a quadrupole toroidal magnetic field[5] for the cases with and without the applied toroidal magnetic field, respectively.

In this paper, it is shown that the flow asymmetry, in particular of the electrons, is associated with the divergence of both the electron parallel and ion perpendicular flows which was previously not accounted for in the resistive (compressible)[6] and collisionless (incompressible)[1-3] theories. This asymmetric solution has an important consequence for the magnetic reconnection processes since it allows substantial density inhomogeneity and toroidal magnetic field within the current sheet which prohibit its collapse by pressure balance[7]. This new evidence of collisionless magnetic reconnection alters the parametric dependence of the reconnection rate. The major results are a rather weak dependence on the ion inertia and applied toroidal magnetic field compared to the previous MHD studies, and a considerable reduction of the reconnection rate for an ion Larmor radius comparable to the ion skin depth.

The outline of this paper will be the following. In Sec.2, the numerical method and initial setup of the macro-particle simulations are mentioned. Simulation results are shown in the next two sections, with new and qualitative features of collisionless magnetic reconnection in Sec.3 and parametric dependences in Sec.4. A brief conclusion of the simulations will be made in Sec.5.

§2. Simulation Method and Initial Setup

The macro-particle code to be adopted in this study is the low-frequency, large spatial-scale simulation technique[8] which has both the full-kinetic and electron drift-kinetic versions in two-dimensional coordinate space. In both codes, the Maxwell equations are solved for the electromagnetic field,

$$(\partial \mathbf{E}/\partial t)^{n+1/2} = c\nabla \times \mathbf{B}^{n+\alpha} - 4\pi \mathbf{J}^{n+\alpha}, \tag{1}$$

$$(\partial \mathbf{B}/\partial t)^{n+1/2} = -c\nabla \times \mathbf{E}^{n+\alpha}, \tag{2}$$

$$\nabla \cdot \mathbf{E}^{n+1} = 4\pi\rho^{n+1}, \tag{3}$$

$$\nabla \cdot \mathbf{B}^{n+1} = 0, \tag{4}$$

where $\mathbf{E}$ and $\mathbf{B}$ are the electric and magnetic fields, respectively, $\mathbf{J}$ and ρ the current and charge densities. The superscripts stand for the time level of each quantity in the unit Δt, and the constant $\alpha > \frac{1}{2}$ gives time-implicitness which serves to filter out high-frequency components of the electromagnetic oscillations with $\omega\Delta t \geq O(1)$, where ω is their characteristic frequency and Δt is a time step. The equations of motion for each particle are the Newton-Lorentz equations,

$$(d\mathbf{x}_j/dt)^{n+1/2} = \mathbf{v}_j^{n+1/2}, \tag{5}$$

$$(d\mathbf{v}_j/dt)^{n+1/2} = (e_j/m_j)[\mathbf{E}^{n+\alpha} + (\mathbf{v}_j/c)^{n+1/2} \times \mathbf{B}^{n+\alpha}]. \tag{6}$$

When the electrons are well magnetized, the drift-kinetic equations are used,

$$(d\mathbf{x}_j/dt)^{n+1/2} = [v_{\|j}^{n+1/2}\mathbf{b}^{n+\alpha} + \mathbf{v}_{\perp j}^{n+\alpha}], \tag{7}$$

$$(dv_{\|j}/dt)^{n+1/2} = (-e/m_e)E_{\|}^{n+\alpha} - (\mu_j/m_e)\nabla_{\|}B^{n+\alpha}. \tag{8}$$

In the equations, $\mathbf{x}_j$ and $\mathbf{v}_j$ are the position and 3-D velocity of each particle, respectively, $v_{\|j}$, $\mathbf{v}_{\perp j}$ the parallel and perpendicular (guiding-center) velocities of the j-th particle where $\mathbf{v}_{\perp j}$ includes the $E \times B$ and magnetic drifts; magnetization current is added to $\mathbf{J}$ in Eq.(1). $\mathbf{b}$ is the unit vector along the magnetic field, e_j, m_j and μ_j the electric charge, mass and magnetic moment, respectively. It is remarked that the Poisson equation Eq.(3) ensures proper charge neutrality in the two-component plasma[5]

since $\alpha \neq \frac{1}{2}$ in Eq.(1). Also, we note that the electron inertia term is properly retained in the parallel motion in Eq.(8).

A homogeneous charge-neutral plasma is initialized with the same number of ions and electrons (64 ions/cell) in a doubly-periodic Cartesian system (x, z). Three components of the particle velocity are generated with a Boltzmann distribution of given temperatures. The ions located in the core of the flux bundles are given an initial drift toward the positive y-direction to produce a pair of flux bundles. The system size is $L_x = 400c/\omega_{pe}$ and $L_z = 300c/\omega_{pe}$. We use a non-equidistant grid in the x direction, with $\Delta x \cong 0.55c/\omega_{pe}$ in the central region and $\Delta x \cong 1.6c/\omega_{pe}$ in the outer region, and $\Delta z \cong 4.1c/\omega_{pe}$ in the z-direction. It should be noted that particle simulations have a reasonable resolution even with fewer grid points because the current and charge are carried by solid Lagrangian particles[9]. The physical parameters are: the mass ratio $m_i/m_e = 25-200$, the temperature ratio $T_i/T_e = 1/8-49$, and the strength of the ambient toroidal magnetic field (y-direction) $\omega_{ce}^{(0)}/\omega_{pe} = 0-1$. The electron beta value is fixed to $\beta_e = 8\pi nT_e/B_0^2 = 0.04$, except for the runs in Sec.4 with different values of the applied toroidal magnetic field. The time step is $\Delta t/\tau_A \cong 10^{-2}$, with τ_A the poloidal Alfven time for half the initial separation of the flux bundles. The parameters for the standard run described in detail below are: $m_i/m_e = 100$, $T_i/T_e = 1$ and $\omega_{ce}^{(0)}/\omega_{pe} = 1$. (Toroidal and poloidal stand for the y- and (x, z) components, respectively.)

§3. Asymmetric Flows and Micro-Structure of Current Layer

Figure 1 illustrates the time development of the poloidal flux function Ψ which is related to the poloidal magnetic field by $\mathbf{B}_p = \nabla \times (\Psi\hat{y})$. An elongated current sheet with large negative current density ($J_y < 0$) is formed between the flux bundles. Magnetic reconnection proceeds most rapidly at the time $t \cong 1.9\tau_A$ shown in Fig.1(b). At late times the reconnection process is slowed down due to the repulsive force of the surrounding reconnected field. Figure 2 are the enlargements of the plasma quantities in the square region denoted in Fig.1(b). The poloidal current $J_p^{(s)}$, especially that of the electrons in Fig.2(a), shows a significant up/down asymmetry; the adjacent tips of

the expansion fans are staggered and shift downward and upward in the left and right-half planes, respectively. A slight asymmetry is also seen in the ion poloidal current of Fig.2(b).

Since the poloidal plasma flow mostly consists of the $E \times B$ drift in the presence of the ambient magnetic field[4], we subtract that part $q_s n_s V_E$ from the electron and ion currents to obtain $\delta \mathbf{J}_p^{(s)}$, where $V_E = c\mathbf{E} \times \mathbf{B}/B^2$ and q_s, n_s are the charge and number density of either electrons or ions. It is quite interesting that there is a non-vanishing poloidal component in $\delta \mathbf{J}_p^{(s)}$ both for the electrons and ions shown in the middle panels of Fig.2. The electron component $\delta \mathbf{J}_p^{(e)}$ is quite asymmetric which directs leftward (rightward) in the upper (lower) half-plane. Also, it is stronger on the flanks than at the center of the current sheet. (Magnetization current has been subtracted from the electrons in Fig.2(a).) The residual component for the ions $\delta \mathbf{J}_p^{(i)}$, which mostly consists of magnetization current due to the quadrupole inhomogeneous density to be mentioned later, is rather symmetric.

The origin of the asymmetry in Fig.2, which was not observed in the previous MHD studies, is disclosed in the following manner. First, we note that the magnetic field line, which is a sum of the toroidal field ($B_t^{(0)} > 0$) and the poloidal field represented by the contours of the poloidal flux function in Fig.3(c), has certain angles with respect to the (x, z) plane; it inclines up-rightward and down-leftward in the upper and lower sides of the neutral line, respectively. Thus, the parallel electric field $E_\parallel = (\mathbf{E} \cdot \mathbf{B})/B^2$ in Fig.3(a), which is almost the projection of the toroidal electric field E_y onto the magnetic field line. can accelerate the light-mass electrons *poloidally* rightward and leftward in the upper and lower half-planes, respectively. Indeed, not only the $E_\parallel < 0$ region superimposes quite well with the region where the asymmetric current exists, but these directions coincide with those of the asymmetric poloidal current shown in Fig.2(a). As it takes a finite time for the incoming electrons into the current sheet to get accelerated, $\delta \mathbf{J}_p^{(e)}$ should be stronger on the flanks of the current sheet than at the X-point, as has been mentioned with Fig.2.

Moreover, as the region of the parallel electric field $E_\parallel < 0$ is spatially limited (Fig.3(a)), the electrons are accelerated along the field line and accumulate at the

boundary of such region. This results in substantial quadrupole density hills and holes in the current sheet both for the electrons and ions, $\delta n_s/n_0 \sim 0.3$, as seen in the bottom panels of Fig.2.

The present picture of the asymmetry in terms of the electron parallel motion under the influence of the toroidally induced electric field is proved as follows. First, the magnetic drifts of electrons are not playing a role to the 0-th order because we obtain a similar poloidal asymmetry without them, as depicted in Fig.4(b). Second, when the direction (sign) of the ambient toroidal magnetic field is reversed, that of the parallel electric field is reversed. If the parallel electric field has something to do, the up/down asymmetry of the parallel current $\delta \mathbf{J}_p^{(e)}$ in Fig.2 should be reversed, which is really the case as demonstrated in Fig.4(a). Third, the parallel motion is certainly a key ingredient because the isolated poloidal flux does not merge only without the electron *poloidal* displacement due to the parallel motion in a tiny region including the X-point. This evidence also eliminates a possibility that the present results are numerical fictions.

The cause of the discrepancy between the previous collisionless MHD theories and the present particle simulation is located in the MHD's assumption that the plasma motion be incompressible (divergence-free) everywhere for each of the electron and ion species. This assumption allows the convenient use of the stream function for the plasma flow, however, it rules out non-symmetric solutions. Figure 4(c) evidently disproves this assumption even in the presence of a strong ambient magnetic field. The divergence of the current density is found to be significant in the current sheet, $|\nabla \cdot \mathbf{J}^{(s)}|/|\mathbf{J}^{(s)}| \sim 0.05(\omega_{pe}/c)$. Interestingly, the divergence of the electron current arises from the parallel motion, $\nabla \cdot \mathbf{J}^{(e)} \cong \nabla_{\parallel} \cdot \mathbf{J}_{\parallel}^{(e)}$. On the other hand, for the ion species with large mass, we observe the two-dimensional nature $\nabla \cdot \mathbf{J}^{(i)} \cong \nabla_{\perp} \cdot \mathbf{J}_{\perp}^{(i)}$, owing to the polarization drift $v_{P\perp} \propto m_i$. These divergences of the current density are directly linked to the density inhomogeneity in the current layer. It should be noted that the divergence of the total current vanishes, $\nabla \cdot (\mathbf{J}^{(e)} + \mathbf{J}^{(i)}) \cong 0$, as it should be in a plasma for scale lengths exceeding the Debye length.

On top of the large-scale asymmetry, the magnetization current due to the quadrupole

density hills and holes, $v_n = (v_\perp^2/2\omega_{ce})(\nabla n/n)$ with $\nabla n/n \sim 1/\ell_B$, generates the small-scale localized current and toroidal magnetic field of the same quadrupole configuration (Fig.3(d)). The gradient-B current is two orders of magnitude smaller than the magnetization current, since $\nabla B/B \sim (B_p/B_t)^2/2\ell_B$. An appreciable localized change in the plasma pressure arises from that in the plasma density depicted in Fig.2.

As has been seen in Figures 2 and 3, the finite-thickness current sheet has the internal structure which is shown to be maintained by pressure balance between the plasma and magnetic pressures. Both the asymmetric current due to the parallel electron motion which encircles the periphery of the current sheet and the localized quadrupole magnetization current (Fig.2) generate the perturbed toroidal magnetic field within the current sheet. The larger-scale perturbed field has a sign that always enhances the original toroidal field there, hence the toroidal magnetic pressure. Also, the localized toroidal magnetic and plasma pressures are large enough to achieve pressure balance with the poloidal magnetic pressure outside the current sheet, as shown in Fig.4(d).

§4. Parametric Dependences

(a) Ion Inertia and Larmor Radius Effects

After having demonstrated new and novel features of collisionless magnetic reconnection, we proceed to investigate the reconnection speed using the same macro-particle simulation code. The reconnection rate is defined by measuring the amount of decrease in the isolated poloidal flux contained in either of the flux bundles $\Delta\Psi$ over the time interval $\Delta\tau$ from the onset time; the interval always includes the most rapid phase of reconnection and is typically $\Delta\tau = 1.5\tau_A$. This definition is superior to merely reading off the gradient of the isolated poloidal flux since it integrates out the deviations arising from time-and-space non-smoothness in particle simulations. In what follows, we briefly summarize the recent simulation results in which the mass dependence $(m_i/m_e)^{1/2}$ is absorbed in the Alfven time.

Figure 5(a) shows the dependence of the reconnection rate on the ion inertia; the mass ratio (m_i/m_e) is varied by fixing the electron mass. There is a general tendency

of increasing reconnection rate with the ion mass. The dependence is mild unless the ion Larmor radius ρ_i is comparable to the ion skin depth, $\rho_i \sim c/\omega_{pi} \propto (m_i/m_e)^{1/2}$ ($c/\omega_{pi} = 5c/\omega_{pe}$ for $m_i/m_e = 25$), below which the ion motion is considered to be decoupled from the electrons[3]. These results qualitatively agree with the previous MHD studies, but quantitatively are less sensitive to the ion inertia. The finding that the current sheet thickness for these runs does not vary as much as in the MHD studies is in line with the mild dependence.

A drastic reduction of the reconnection rate is observed in Fig.5(b), which is expected to be the finite Larmor radius (FLR) effect of the ions. The dependence on the ion Larmor radius for the $m_i/m_e = 100$ case in Fig.5(b) ($c/\omega_{pi} = 10c/\omega_{pe}$) and the deviation of the two lines for $m_i/m_e \leq 50$ in Fig.5(a) show that the reconnection rate is the decreasing function of the ion Larmor radius divided by the ion skin depth,

$$d\Psi/d\tau \;=\; F(\rho_i/(c/\omega_{pi})^{\nu}), \tag{9}$$

with $\nu \cong 2.7$ and the F profile given by Fig.5(b). The ion mass dependence in Eq.(9) is $F(m_i^{(1-\nu)/2})$. We note that for the large ion Larmor radius case the ions do not closely follow the $E \times B$ drift by which the electron poloidal motion is well described, which might be beyond the MHD theory with kinetic corrections[10].

(b) Compressible Effects under Weak Magnetic Field

A dependence on the strength of the applied toroidal magnetic field is another issue of interest. The simulation results using the full-kinetic code are also plotted for the two cases of the magnetic field ratio, $B_t^{(0)}/B_p \cong 0$ and 1 in Fig.5(a) ($m_i/m_e = 100$). Under the intermediate toroidal magnetic field $B_t \sim B_p$, the plasma flows are still asymmetric. But, the whole current sheet is compressed to form a high-density channel, $<n_s>/n_0 \sim 1.5$, with widely-open expansion fans characteristic of the X-point. For the $B_t^{(0)}/B_p \cong 1$ case ($\rho_i \cong 2c/\omega_{pe}$), the reconnection rate increases by 20 percent (open square).

When the ambient magnetic field is not applied, the plasma flow becomes symmetric as shown in Fig.6 of Ref.5. However, the neutral sheet is more densely compressed,

$< n_s > / n_0 \sim 2.1$, and the reconnection rate further increases (filled square). The experimental formula of the current sheet density is,

$$< n_s > \sim n_0(2+\epsilon)/(1+\epsilon) \tag{10}$$

with $\epsilon = B_t/B_p$. From the flux balance, the reconnection rate should scale as,

$$d\Psi/d\tau \propto < n_s > v_A/n_0 \sim \sqrt{< n_s >}, \tag{11}$$

which roughly agrees with the observation in Fig.5(a).

Finally, a run with half the system size reveals the role of the electron inertia (the electron thermal speed is also halved to keep the beta value constant). The reconnection rate does increase as shown by the + symbol in Fig.5(a). Thus. it is concluded that, although the collisionless reconnection rate is principally determined by the ions with large inertia, the effects of electron parallel motion due to the finite inertia $m_e \neq 0$ cannot be ignored.

§5. Conclusion

It has been shown for the first time in the present study that the electron parallel motion manifested by the flow asymmetry plays an important role in collisionless magnetic reconnection. Namely, the parallel motion of the light-mass electrons, which is a natural consequence of removing the symmetric flow assumption around the X-point, causes divergence of the plasma flows in the electron current layer and results in the thick current sheet. Thus, the parametric dependences of collisionless reconnection rate become mild compared to the collisionless MHD studies assuming the symmetric flows.

The collisionless reconnection rate has been shown to be principally determined by the ion inertia which is, however, coupled and affected by the electron parallel motion. Finiteness of the ion Larmor radii has been found to cut the reconnection rate drastically for the Larmor radii comparable to the ion skin depth. On the other hand, the plasma compressibility under the weak toroidal magnetic field has been shown to increase the reconnection rate, as in the resistive case. Finally, a coupling with the three dimensional effects will be an interesting problem in the future.

References

1. J.F.Drake and R.G.Kleva, Phys.Rev.Lett., 66, 1458 (1991).
2. M.Ottaviani and F.Porcelli, Phys.Rev.Lett., 71, 3802 (1993).
3. D.Biskamp and J.F.Drake, Phys.Rev.Lett., 75, 3850 (1995).
4. M.Tanaka, Phys.Plasmas, 2, 2920 (1995).
5. M.Tanaka, Comput.Phys.Commun., 87, 117 (1995).
6. A.Bhattachargee, F.Brunel, and T.Tajima, Phys.Fluids, 26, 3332 (1983).
7. M.Tanaka, Bull.Amer.Phys.Soc., 40, 1877 (1995).
8. M.Tanaka, J.Comput.Phys., 107, 124 (1993); ibid., 79, 209 (1988).
9. D.Sulsky, S-J.Zhou, and H.L.Schreyer, Comput.Phys.Commun., 87, 236 (1995).
10. L.Zhakarov, B.Rogers, and S.Miglioulo, Phys.Fluids B5, 2498 (1993).

Figure Captions

Figure 1. Time development of the poloidal flux function for the standard run in (a) the equilibrium state at $t = 0.75\tau_A$, (b) the most rapid phase of reconnection at $t \cong 1.9\tau_A$, and (c) at $t = 2.5\tau_A$.

Figure 2. The enlargements of the poloidal current $J_p^{(s)}$, the residual current with the $E \times B$ component subtracted $\delta J_p^{(s)}$, and the number density n_s in the square region denoted in Fig.1(b), from top to bottom, respectively. The column (a) is for the electrons and (b) for the ions. (Magnetization current has been subtracted in (a), and $\delta n_s/n_0 \sim 0.3$.)

Figure 3. The enlargements of (a) the parallel electric field $E_\parallel$, (b) the electrostatic potential φ, (c) the poloidal flux function Ψ, and (d) the perturbed toroidal magnetic field δB_t at $t \cong 1.9\tau_A$ of the standard run. The maximum strengths are $E_\parallel \sim 7.4 \times 10^{-4}$, $\varphi \sim 0.16$, $\Psi \sim 8.7$, and $\delta B_t \sim 2.4 \times 10^{-2}$.

Figure 4. The enlargements of the electron poloidal current for (a) the $B_t^{(0)} < 0$ run, and (b) the run ignoring the electron magnetic drifts. (c) The divergence of the electron current, and (d) the crosscut of the plasma and magnetic pressures vertically through the current sheet at $z = 0.41L_z$ for the standard run.

Figure 5. The parametric dependences of the reconnection rate on (a) the ion mass ($\rho_i = 1$, $2c/\omega_{pe}$), and (b) the ion Larmor radius ($m_i/m_e = 100$, fixed). In (a), also the reconnection rates for the applied toroidal magnetic field of $B_t^{(0)} = 0$, 0.2 and for half the system size are plotted with squares and the + symbol, respectively.

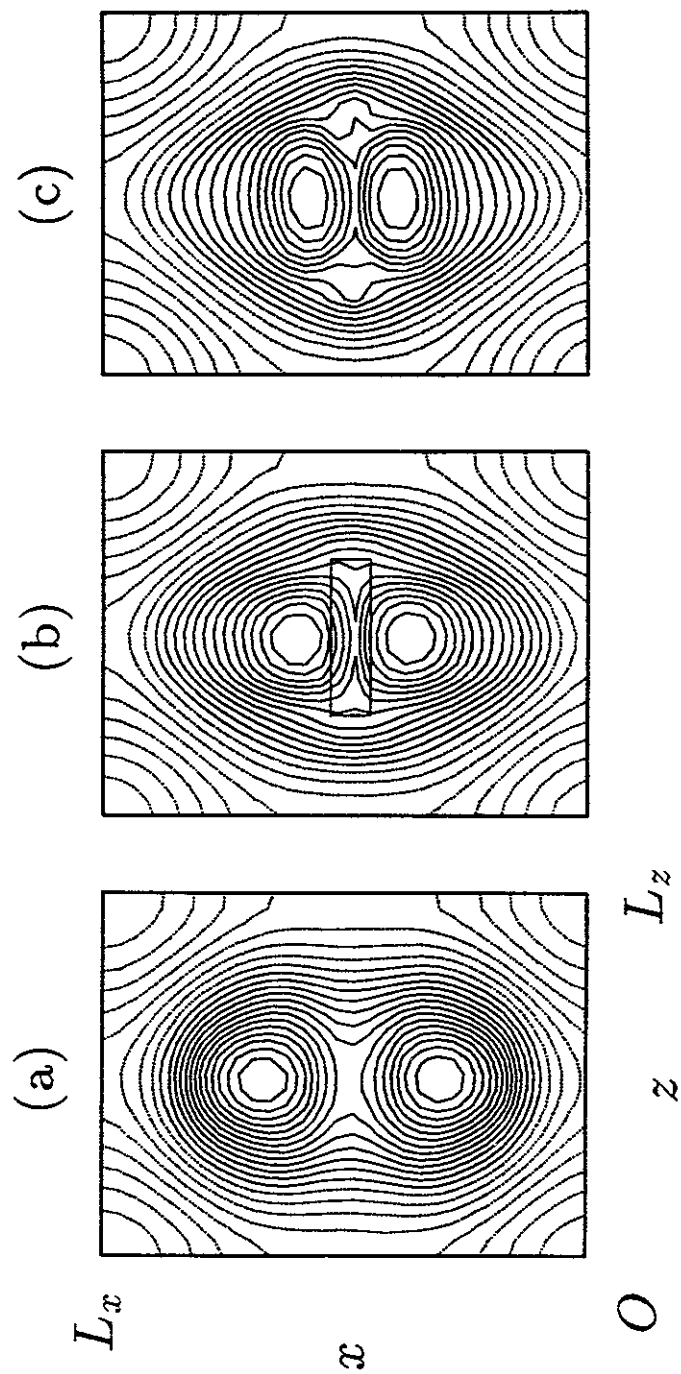

Figure 1.

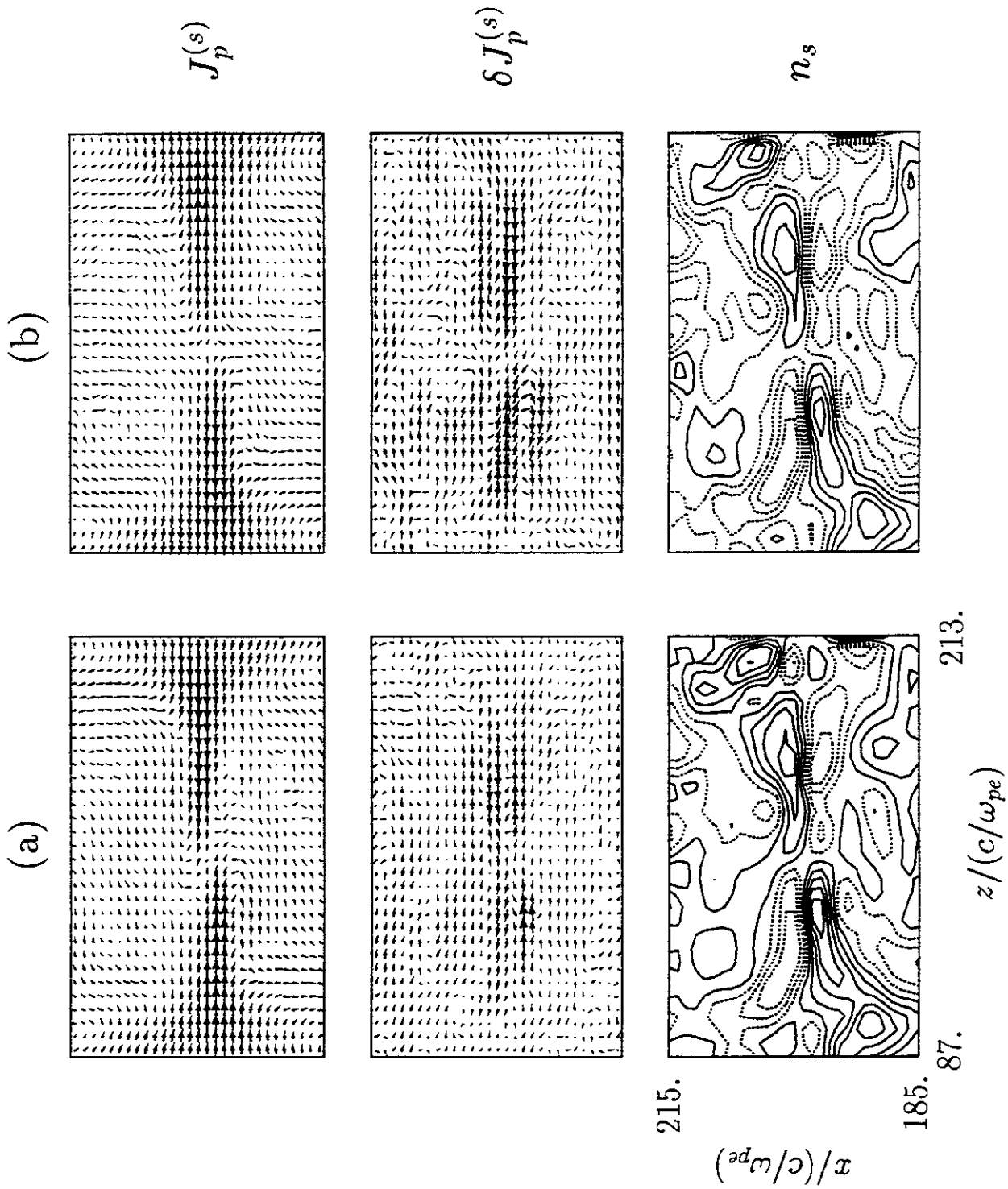

Figure 2.

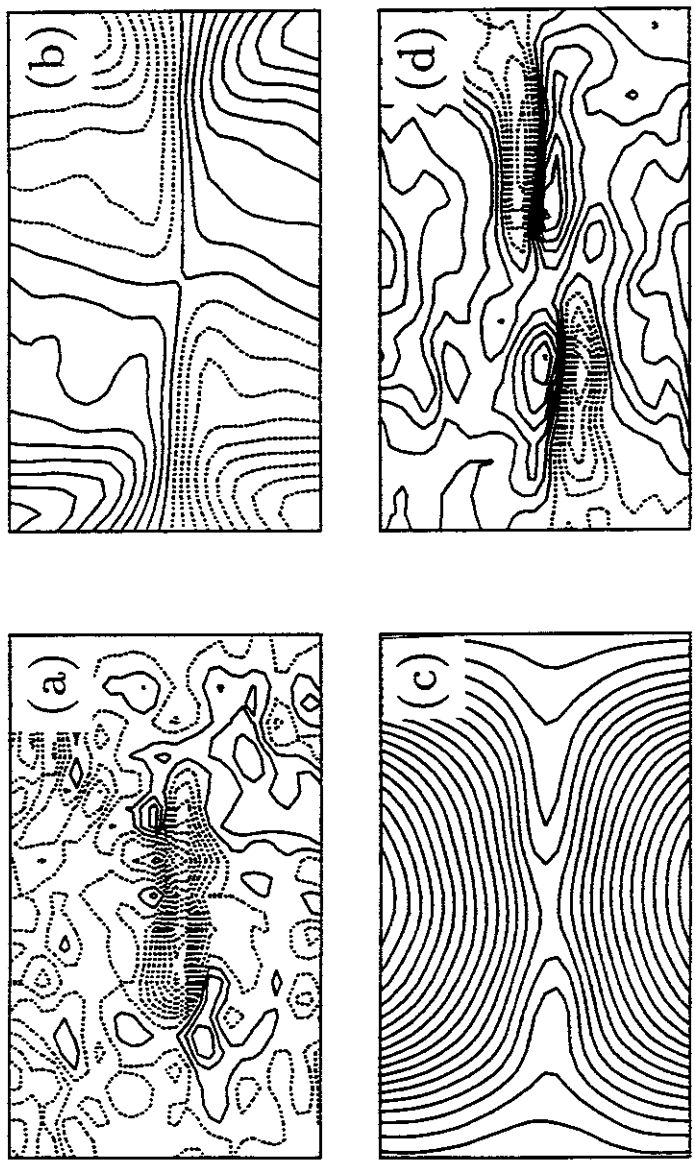

Figure 3.

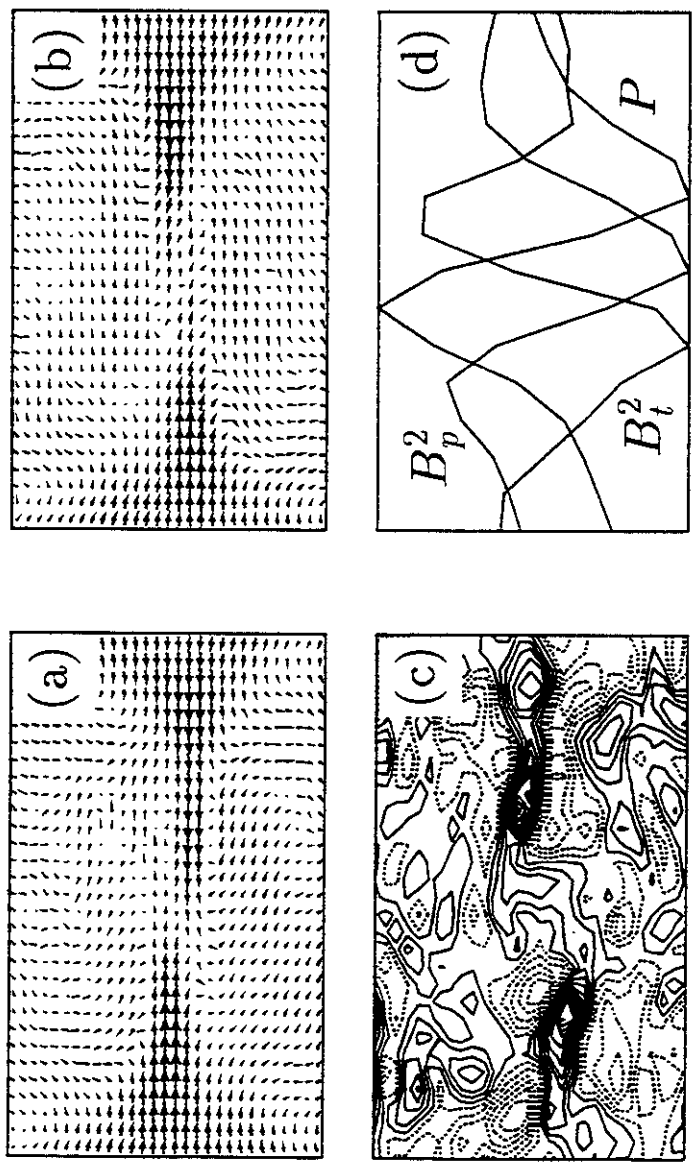

Figure 4.

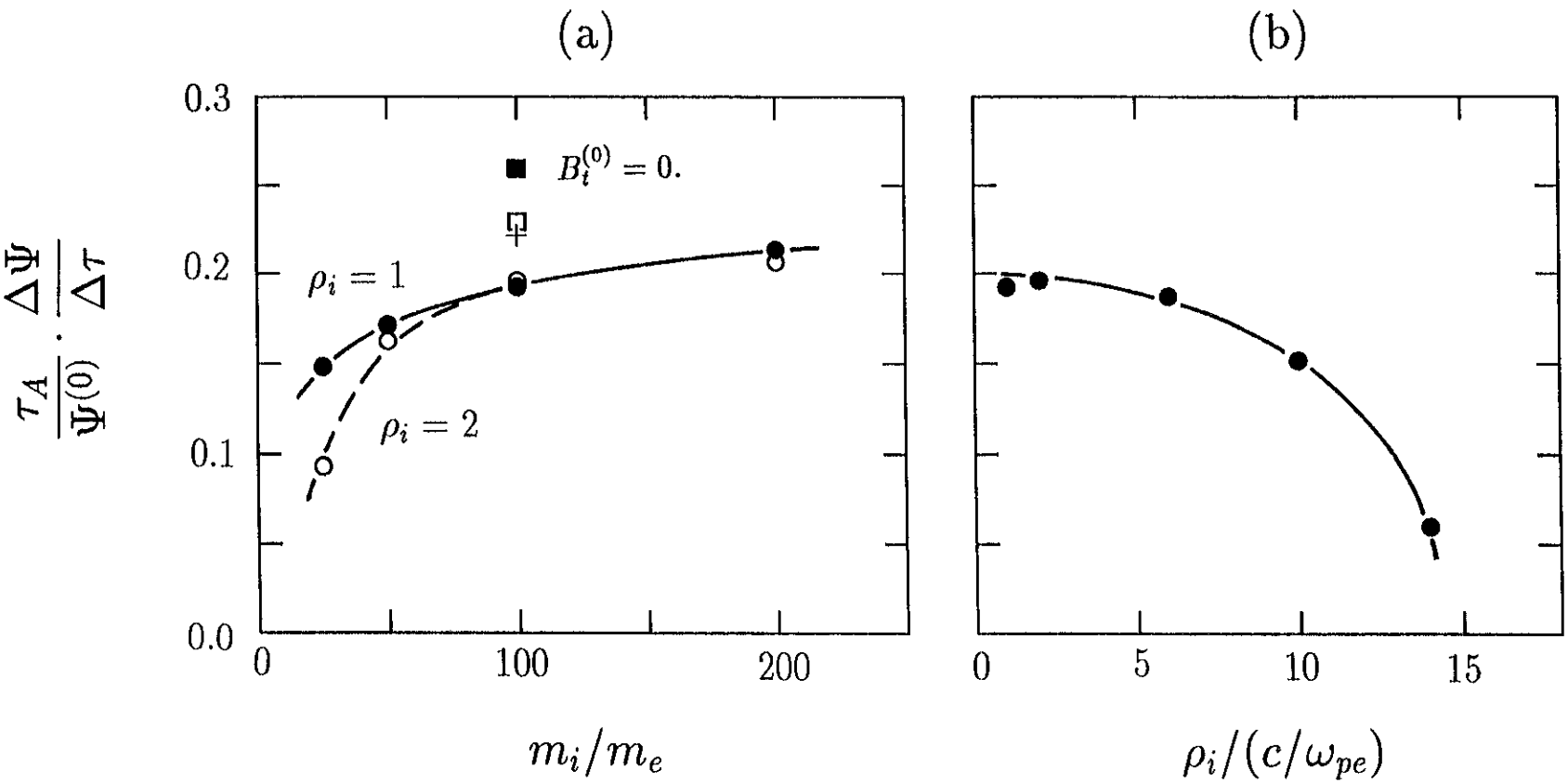
(a)
(b)
0.3
0.2
0.1
0.0
$B_i^{(0)} = 0.$
$\rho_i = 1$
$\rho_i = 2$
0
100
200
0
5
10
15
$\frac{\tau_A}{\Psi(0)} \cdot \frac{\Delta\Psi}{\Delta\tau}$
m_i/m_e
$\rho_i/(c/\omega_{pe})$

Figure 5.

Recent Issues of NIFS Series

NIFS-358 M. Ida and T. Yabe,
Implicit CIP (Cubic-Interpolated Propagation) Method in One Dimension; May 1995

NIFS-359 A. Kageyama, T. Sato and The Complexity Simulation Group,
Computer Has Solved A Historical Puzzle: Generation of Earth's Dipole Field; June 1995

NIFS-360 K. Itoh, S.-I. Itoh, M. Yagi and A. Fukuyama,
Dynamic Structure in Self-Sustained Turbulence; June 1995

NIFS-361 K. Kamada, H. Kinoshita and H. Takahashi,
Anomalous Heat Evolution of Deuteron Implanted Al on Electron Bombardment; June 1995

NIFS-362 V.D. Pustovitov,
Suppression of Pfirsch-schlüter Current by Vertical Magnetic Field in Stellarators; June 1995

NIFS-363 A. Ida, H. Sanuki and J. Todoroki
An Extended K-dV Equation for Nonlinear Magnetosonic Wave in a Multi-Ion Plasma; June 1995

NIFS-364 H. Sugama and W. Horton
Entropy Production and Onsager Symmetry in Neoclassical Transport Processes of Toroidal Plasmas; July 1995

NIFS-365 K. Itoh, S.-I. Itoh, A. Fukuyama and M. Yagi,
On the Minimum Circulating Power of Steady State Tokamaks; July 1995

NIFS-366 K. Itoh and Sanae-I. Itoh,
The Role of Electric Field in Confinement; July 1995

NIFS-367 F. Xiao and T. Yabe,
A Rational Function Based Scheme for Solving Advection Equation; July 1995

NIFS-368 Y. Takeiri, O. Kaneko, Y. Oka, K. Tsumori, E. Asano, R. Akiyama, T. Kawamoto and T. Kuroda,
Multi-Beamlet Focusing of Intense Negative Ion Beams by Aperture Displacement Technique; Aug. 1995

NIFS-369 A. Ando, Y. Takeiri, O. Kaneko, Y. Oka, K. Tsumori, E. Asano, T. Kawamoto, R. Akiyama and T. Kuroda,
Experiments of an Intense H- Ion Beam Acceleration; Aug. 1995

NIFS-370 M. Sasao, A. Taniike, I. Nomura, M. Wada, H. Yamaoka and M. Sato, *Development of Diagnostic Beams for Alpha Particle Measurement on ITER*; Aug. 1995

NIFS-371 S. Yamaguchi, J. Yamamoto and O. Motojima; *A New Cable -in conduit Conductor Magnet with Insulated Strands*; Sep. 1995

NIFS-372 H. Miura, *Enstrophy Generation in a Shock-Dominated Turbulence*; Sep. 1995

NIFS-373 M. Natsir, A. Sagara, K. Tsuzuki, B. Tsuchiya, Y. Hasegawa, O. Motojima, *Control of Discharge Conditions to Reduce Hydrogen Content in Low Z Films Produced with DC Glow;* Sep. 1995

NIFS-374 K. Tsuzuki, M. Natsir, N. Inoue, A. Sagara, N. Noda, O. Motojima, T. Mochizuki, I. Fujita, T. Hino and T. Yamashina, *Behavior of Hydrogen Atoms in Boron Films during H_2 and He Glow Discharge and Thermal Desorption;* Sep. 1995

NIFS-375 U. Stroth, M. Murakami, R.A. Dory, H. Yamada, S. Okamura, F. Sano and T. Obiki, *Energy Confinement Scaling from the International Stellarator Database*; Sep. 1995

NIFS-376 S. Bazdenkov, T. Sato, K. Watanabe and The Complexity Simulation Group, *Multi-Scale Semi-Ideal Magnetohydrodynamics of a Tokamak Plasma;* Sep. 1995

NIFS-377 J. Uramoto, *Extraction of Negative Pionlike Particles from a H2 or D2 Gas Discharge Plasma in Magnetic Field;* Sep. 1995

NIFS-378 K. Akaishi, *Theoretical Consideration for the Outgassing Characteristics of an Unbaked Vacuum System*; Oct. 1995

NIFS-379 H. Shimazu, S. Machida and M. Tanaka, *Macro-Particle Simulation of Collisionless Parallel Shocks*; Oct. 1995

NIFS-380 N. Kondo and Y. Kondoh, *Eigenfunction Spectrum Analysis for Self-organization in Dissipative Solitons;* Oct. 1995

NIFS-381 Y. Kondoh, M. Yoshizawa, A. Nakano and T. Yabe, *Self-organization of Two-dimensional Incompressible Viscous Flow in a Friction-free Box;* Oct. 1995

NIFS-382 Y.N. Nejoh and H. Sanuki,

The Effects of the Beam and Ion Temperatures on Ion-Acoustic Waves in an Electron Beam-Plasma System; Oct. 1995

NIFS-383 K. Ichiguchi, O. Motojima, K. Yamazaki, N. Nakajima and M. Okamoto
Flexibility of LHD Configuration with Multi-Layer Helical Coils;
Nov. 1995

NIFS-384 D. Biskamp, E. Schwarz and J.F. Drake,
Two-dimensional Electron Magnetohydrodynamic Turbulence; Nov. 1995

NIFS-385 H. Kitabata, T. Hayashi, T. Sato and Complexity Simulation Group,
Impulsive Nature in Collisional Driven Reconnection; Nov. 1995

NIFS-386 Y. Katoh, T. Muroga, A. Kohyama, R.E. Stoller, C. Namba and O. Motojima,
Rate Theory Modeling of Defect Evolution under Cascade Damage Conditions:The Influence of Vacancy-type Cascade Remnants and Application to the Defect Production Chracterization by Microstructural Analysis; Nov. 1995

NIFS-387 K. Araki, S. Yanase and J. Mizushima,
Symmetry Breaking by Differential Rotation and Saddle-node Bifurcation of the Thermal Convection in a Spherical Shell; Dec. 1995

NIFS-388 V.D. Pustovitov,
Control of Pfirsch-Schlüter Current by External Poloidal Magnetic Field in Conventional Stellarators: Dec. 1995

NIFS-389 K. Akaishi,
On the Outgassing Rate Versus Time Characteristics in the Pump-down of an Unbaked Vacuum System; Dec. 1995

NIFS-390 K.N. Sato, S. Murakami, N. Nakajima, K. Itoh,
Possibility of Simulation Experiments for Fast Particle Physics in Large Helical Device (LHD); Dec. 1995

NIFS-391 W.X.Wang, M. Okamoto, N. Nakajima, S. Murakami and N. Ohyabu,
A Monte Carlo Simulation Model for the Steady-State Plasma in the Scrape-off Layer; Dec. 1995

NIFS-392 Shao-ping Zhu, R. Horiuchi, T. Sato and The Complexity Simulation Group,
Self-organization Process of a Magnetohydrodynamic Plasma in the Presence of Thermal Conduction; Dec. 1995

NIFS-393 M. Ozaki, T. Sato, R. Horiuchi and the Complexity Simulation Group
Electromagnetic Instability and Anomalous Resistivity in a Magnetic Neutral Sheet; Dec. 1995

NIFS-394 K. Itoh, S.-I Itoh, M. Yagi and A. Fukuyama,

Subcritical Excitation of Plasma Turbulence; Jan. 1996

NIFS-395 H. Sugama and M. Okamoto, W. Horton and M. Wakatani,
Transport Processes and Entropy Production in Toroidal Plasmas with Gyrokinetic Eletromagnetic Turbulence; Jan. 1996

NIFS-396 T. Kato, T. Fujiwara and Y. Hanaoka,
X-ray Spectral Analysis of Yohkoh BCS Data on Sep. 6 1992 Flares - Blue Shift Component and Ion Abundances -; Feb. 1996

NIFS-397 H. Kuramoto, N. Hiraki, S. Moriyama, K. Toi, K. Sato, K. Narihara, A. Ejiri, T. Seki and JIPP T-IIU Group,
Measurement of the Poloidal Magnetic Field Profile with High Time Resolution Zeeman Polarimeter in the JIPP T-IIU Tokamak; Feb. 1996

NIFS-398 J.F. Wang, T. Amano, Y. Ogawa, N. Inoue,
Simulation of Burning Plasma Dynamics in ITER; Feb. 1996

NIFS-399 K. Itoh, S-I. Itoh, A. Fukuyama and M. Yagi,
Theory of Self-Sustained Turbulence in Confined Plasmas; Feb. 1996

NIFS-400 J. Uramoto,
A Detection Method of Negative Pionlike Particles from a H2 Gas Descharge Plasma; Feb. 1996

NIFS-401 K.Ida, J.Xu, K.N.Sato, H.Sakakita and JIPP TII-U group,
Fast Charge Exchange Spectroscopy Using a Fabry-Perot Spectrometer in the JIPP TII-U Tokamak; Feb. 1996

NIFS-402 T. Amano,
Passive Shut-Down of ITER Plasma by Be Evaporation; Feb. 1996

NIFS-403 K. Orito,
A New Variable Transformation Technique for the Nonlinear Drift Vortex; Feb. 1996

NIFS-404 T. Oike, K. Kitachi, S. Ohdachi, K. Toi, S. Sakakibara, S. Morita, T. Morisaki, H. Suzuki, S. Okamura, K. Matsuoka and CHS group;
Measurement of Magnetic Field Fluctuations near Plasma Edge with Movable Magnetic Probe Array in the CHS Heliotron/Torsatron; Mar. 1996

NIFS-405 S.K. Guharay, K. Tsumori, M. Hamabe, Y. Takeiri, O. Kaneko, T. Kuroda,
Simple Emittance Measurement of H- Beams from a Large Plasma Source; Mar. 1996

NIFS-406 M. Tanaka and D. Biskamp,
Symmetry-Breaking due to Parallel Electron Motion and Resultant Scaling in Collisionless Magnetic Reconnection; Mar. 1996